NANO LETTERS

2004
Vol. 4, No. 7
1313−1318

Microstructure and Interdiffusion of Template-Synthesized Au/Sn/Au Junction Nanowires

Jin-Guo Wang,*,† Ming-Liang Tian,†,‡ Thomas E. Mallouk,†,§ and Moses H. W. Chan†,‡

Materials Research Institute and Center for Nanoscale Science, The Pennsylvania State University, 194 Materials Research Institute Building, University Park, Pennsylvania 16802, Department of Physics, The Pennsylvania State University, 104 Davey Laboratory, University Park, Pennsylvania 16802, and Department of Chemistry, The Pennsylvania State University, 152 Davey Laboratory, University Park, Pennsylvania 16802

Received May 10, 2004

ABSTRACT

Microstructure and interdiffusion of striped Au/ Sn/Au nanowires grown by sequential electrodeposition of Au and Sn in porous polycarbonate membranes were investigated by X-ray diffraction, HRTEM, STEM, EDS, and electrical transport measurements. The Au/Sn junctions were found to contain two intermetallic phases: AuSn, and $AuSn_4$. Mechanisms for the formation of these intermetallic phases and the effect of these phases on the superconductivity of striped nanowires were discussed.

A variety of quasi-one-dimensional nanostructures, which include nanotubes, nanorods, nanowires, and nanobelts, have been synthesized by different techniques. Template synthesis is a versatile and simple approach to the preparation of metallic nanowires and/or nanotubes.[1] Arrays of nanowires are obtained by filling a porous template that contains a large number of straight cylindrical holes with a narrow size distribution.[1−3] Holes can also be filled with two different materials stacked in an alternating fashion to form multilayers.[4−7] Metallic (Au, Ag, Cu, et al.) nanowires are among the most interesting for exploring the fundamental growth mechanisms and physical properties. Metallic nanowires with single crystal and polycrystalline structures have been synthesized by using the template synthetic method.[8−10]

Elemental metals or alloys, which have long been used as interconnect materials in conventional electronic devices, should also be good candidate materials for interconnects in nanodevices of the future. In such interconnects, interfacial transport and reactions at nanojunctions will be very significant due to the increased surface area, and will strongly affect the quality and lifetime of the nanodevices. The interdiffusion of components also affects the electrical transport properties and is important in the failure mechanism of nanowires under current stress. Thus, it is of interest to investigate the interdiffusion between two components in one-dimensional nanostructures. The Au−Sn system is an interesting one to study because interdiffusion is expected to occur at relatively low temperature. Sn-based alloys are also among the most promising lead-free solders, and knowledge of the interfacial reactions between nanoscale Sn solders and electronic substrates is essential.[11] Additionally, Sn nanowires are expected to show confinement effects in superconductivity, such as finite residual resistance at low temperatures.[12−14] Experimental studies have shown that patterned normal metal conducting leads can strongly affect the transport properties of superconducting junctions.[15] Here we report a study of the microstructure of striped Au/Sn/Au nanowires and the effect of the Au/Sn interconnecting junction on their superconductivity.

Striped Au/Sn/Au nanowires were fabricated by electrodepositing metals (Au and Sn) into commercially available polycarbonate membranes (Structure Probe Inc.). The quoted pore diameters and thickness of the membranes were 10−40 nm and 6 μm, respectively, and the pore density was about 6×10^6 pore/cm^2. A glass tube cell with two electrodes was used for electrodeposition, which was carried out potentiostatically at ambient temperature. Au was deposited first using a commercial Orotemp Au plating solution (Technic, Inc.) diluted with the same volume of water. A 0.8 mm diameter Pt wire was used as the anode, and a Au film

* Corresponding author. Tel (814) 865-9285; Fax (814) 863-8561, (814) 863-0637; E-mail: jqw11@psu.edu.
† Materials Research Institute and Center for Nanoscale Science.
‡ Department of Physics.
§ Department of Chemistry.

10.1021/nl0492988 CCC: $27.50
Published on Web 06/10/2004

evaporated on the one side of the polycarbonate membrane served as the cathode. A voltage of −2.3 V was applied between the Au film cathode and the Pt anode. The electrolyte for growing Sn wires was 0.l M aqueous $SnSO_4$, with the pH adjusted to 1 by addition of concentrated H_2SO_4. Pure Sn wire was used as the anode, and the depositing voltage was about −0.8 mV. To increase the wettability of the polycarbonate membrane, a small amount of gelatin was added to both solutions.[8,16,17] The deposition time for each segment of Au−Sn−Au nanowires was, respectively, about 4, 5, and 4 min. During the period when the Sn electrolyte was switched to the Au electrolyte, a negative bias of 0.1 V was applied in order to avoid oxidation of the Sn wires. The nanowires were harvested by dissolving the polycarbonate membrane in dichloromethane and were separated from the solvent by means of a centrifuge. The free-standing nanowires were stored as a suspension in ethyl alcohol.

TEM specimens were prepared by placing a drop of the nanowire suspension on a Lacey carbon grid. Microscopy was performed with a 200 kV JEOL 2010F field-emission TEM, which was equipped with an annular dark field detector, a post-column electron energy loss (EELS) image (Gatan Enfina), and an Oxford energy-dispersive X-ray (EDX) detector. High angular dark field STEM images and EDX analysis were used to identify the intermetallic phases along the length of the Au/Sn/Au nanowires, and the duration of the EDX scans on individual spots was 20−40 s.

Transport measurements were carried out on a Au/Sn/Au nanowire array still in the polycarbonate membrane (40 nm nominal pore diameter) in a two-probe configuration, in which conducting leads were attached on both sides of the membrane. The temperature, which was controlled by a physical properties measurement system (PPMS) (Quantum Design, Inc.), could reach about 0.4 K. The excitation current was about 0.1 μA, far below the critical current of the nanowire array.

Figure 1a shows a low magnification TEM image of Au/Sn/Au nanowires. The nanowires appear uniform at low magnification. An X-ray diffraction pattern from the nanowires within the membranes is shown in Figure 1b. Reflections assigned to the major phases present (Au and Sn) dominate the pattern. In addition, there are several small peaks (indicated by arrows) that can be identified with the AuSn phase, with a hexagonal NiAs-type structure (space group $P6_3/mmc$).

A higher resolution TEM image of a representative Au/Sn/Au nanowire is shown in Figure 2. Both ends of the wire are Au; a 1.5 μm Sn segment is sandwiched between. Locally enlarged images of the both junctions are also shown as insets in Figure 2. It can be clearly seen that the Au segment is polycrystalline and the Sn segment is a single crystal. It is difficult to determine which end of the wire is the "top" and which is the "bottom" after it is released from the membrane, but it is apparent that an intermetallic phase has formed at one of the junctions between Au and Sn. Energy-dispersive X-ray analyses (EDX) were carried out on the spot marked on the TEM image in Figure 2, and the composition of the intermetallic compound in Au/Sn junction was determined

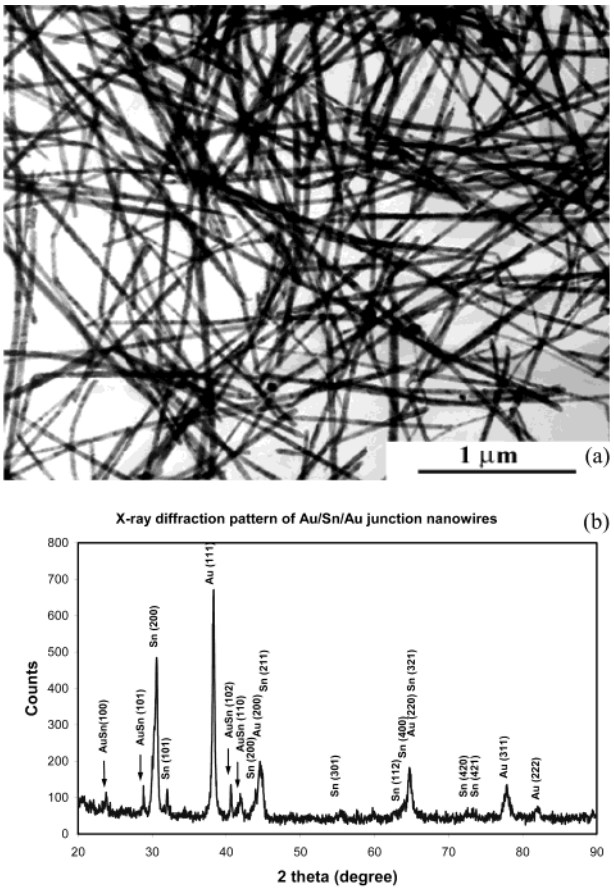

Figure 1. (a) TEM image and (b) X-ray diffraction pattern of Au/Sn/Au nanowires generated by electrochemical deposition.

to be the AuSn phase. It is noteworthy that no intermetallic phase was found at another junction, where pure single-crystal Sn and polycrystalline Au segments connect to each other with a thin intervening layer of Sn oxide, which is also apparent in Figure 2. Here, we will designate the junction that contains intermetallic compounds the "Au/Sn junction" and the junction without intermetallic compounds the "Sn/Au junction".

To evaluate the microstructure and composition of a larger statistical sample of nanowires, the junctions were imaged by using STEM ADF images, which are so-called Z-contrast images combined with selective-area energy-dispersive X-ray analysis (SA-EDX). The intensity of the Z-contrast image is proportional to the square of the atomic number of the sampled atoms. The areas with brighter contrast in the image (Figures 3 and 4) correspond to higher Au content, which have higher average atomic number than areas with higher Sn content. These analyses were carried out on 20 individual nanowires, which were scanned along their length, and spectra were recorded section by section. As expected, the presence of the AuSn intermetallic phase was confirmed for almost all nanowires. In addition, an $AuSn_4$ phase was also found in some junctions and a few of them contained only $AuSn_4$. Two examples are shown in Figures 3 and 4, respectively. Figure 3a shows a STEM ADF image of an Au/Sn/Au nanowire in which the Au/Sn junction contains the two intermetallic compounds AuSn and $AuSn_4$. Again,

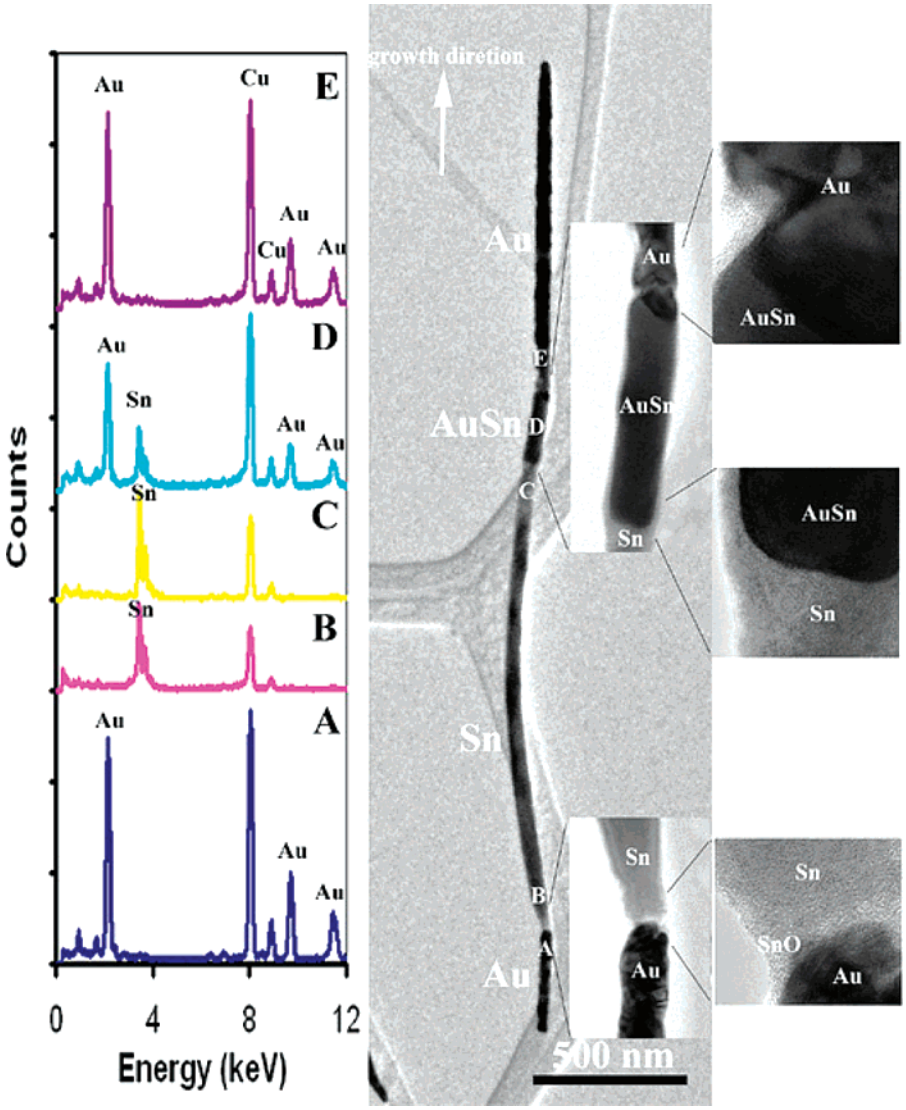

Figure 2. Bright field TEM image and EDX analyses of a representative Au/AuSn/Sn/Au nanowire. Locally enlarged images of the top Au/Sn and bottom Sn/Au junctions are shown as insets. The letters A, B, C, D, and E along the wire axis represent positions at which EDX spectra were recorded. Cu signals originated from the Cu TEM grid.

no intermetallic compound was found at the Sn/Au junction, but a tin oxide layer was observed at the Sn/Au junction. Figure 3b shows the EDX spectra of select spots marked in the Figure 3a. Two intermetallic compounds were clearly identified, and an oxide layer was also observed between $AuSn_4$ and Sn. Figure 4 shows a Au/Sn junction in which only the intermetallic compound $AuSn_4$ was observed. The EDX spectra from selected spots in this segment are displayed in Figure 4b. Although the AuSn4 phase is clearly identified by TEM, there are no peaks corresponding to this phase in the X-diffraction pattern (Figure 1b), presumably because only a small amount of this phase is present. It is also noteworthy that when a nanowire possesses an uneven cross-section, the AuSn compound section is thicker than Au or Sn section.

Previous studies of the diffusion of Au in Sn[18,19] and Sn in Au[20] have revealed that Au diffusion is very rapid in Sn and Sn diffusion is much slower in Au. It has also been found that AuSn is the first compound to form in interdiffusion of Au and Sn.[21] The formation of the AuSn intermetallic phase at the junction is in agreement with the Walser and Bene first phase nucleation rule, which states that the first compound to nucleate in a planar binary reaction couple annealed at low temperature will be the most stable congruently melting compound adjacent to the lowest temperature eutectic on the phase diagram.[22] In the Au−Sn phase diagram, the only congruently melting phase is AuSn. In addition to AuSn, some $AuSn_4$ compound formation at the initial stage of interdiffusion has also been observed.[21] We did not observe Au_5Sn or $AuSn_2$ in our samples, and this is consistent with most of the literature reports on Au−Sn interdiffusion.

There are two major factors that could contribute to the diffusion processes during the electrodeposition process: electric field assisted ion diffusion and thermal diffusion. Considering that there is an applied electric field on the deposited nanowire, the difference in microstructure of the Au/Sn and Sn/Au junctions might come from the migration of Au^+ under the influence of the electric field applied during electrodeposition. Assuming 100% plating efficiency, we can

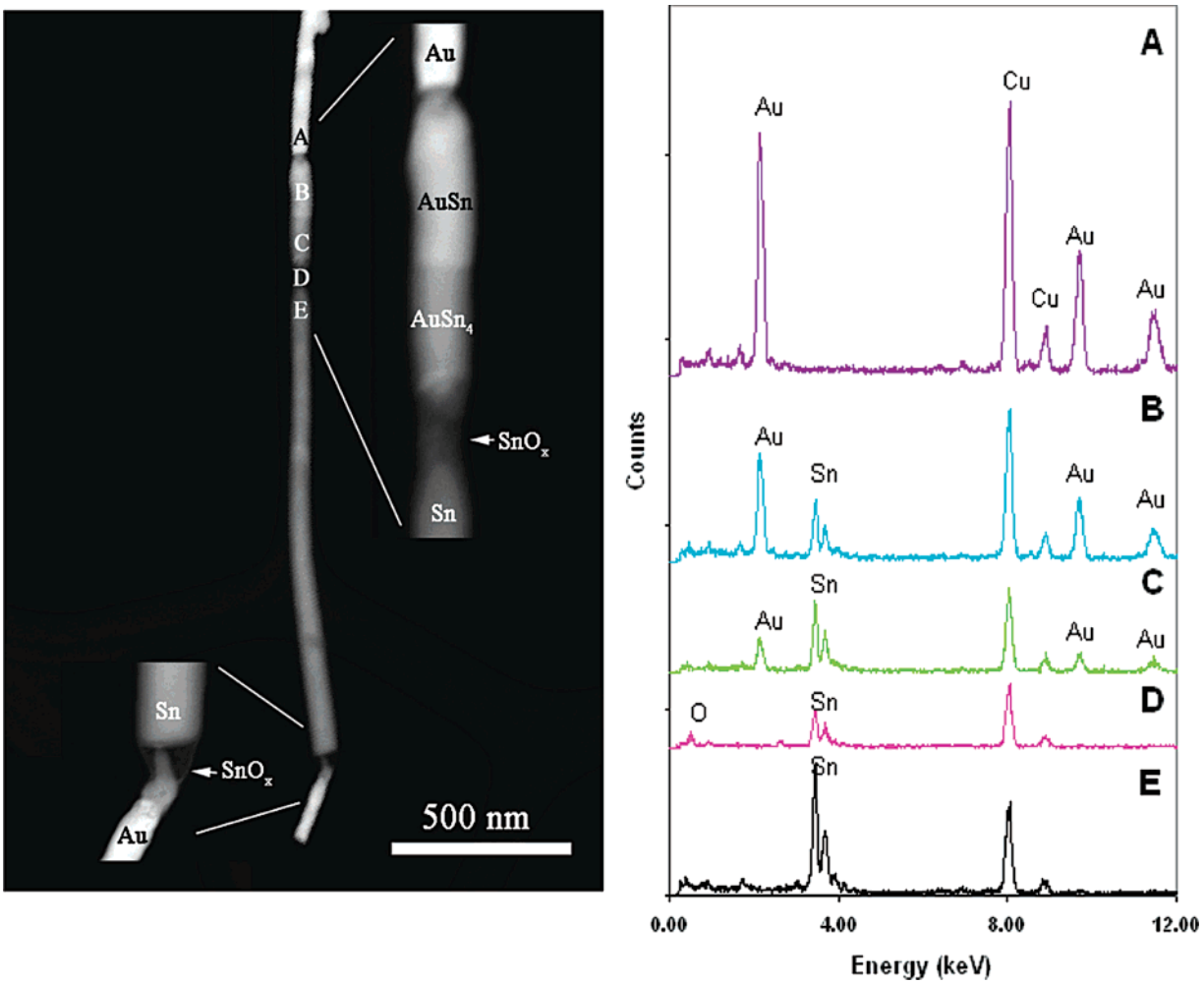

Figure 3. STEM ADF image and EDX analyses of a representative Au/AuSn/$AuSn_4$/Sn/Au nanowire. Locally enlarged images of the top Au/Sn and bottom Sn/Au junctions are shown as insets. The letters A, B, C, D, and E along the wire axis represent positions at which EDX spectra were recorded. Cu signals originated from the Cu TEM grid.

write the current as $i = (L/t)(nFA)(d/\mathrm{FW})$, where L is the segment length, t is the plating time, n is the number of electrons in the plating reaction, F is Faraday's constant, A is the cross sectional area, d is the specific gravity, and FW is the formula weight of the metal. We can multiply i by R/L ($= \rho/A$, where $\rho =$ resistivity) to estimate electric field:

$$E = iR/L = (L/t)(nFd\ \rho/\mathrm{FW})$$

For Au, $L/t = 0.5\ \mu$m/min $= 8.3 \times 10^{-7}$ cm/s; $nF = 96\,500$ coul/mol; $d = 19.5$ g/cm^3; $\rho = 3 \times 10^{-6}$ ohm cm; FW = 197 g/mol. From this one gets $E = 2.4 \times 10^{-8}$ V/cm at a current density $i/A = 8$ mA/cm^2. Because this is an extremely small electric field, we can eliminate the possibility that it affects the diffusion of Au ions significantly.

It has been reported that thermal diffusion of Au in Sn single crystals is very fast.[18] This bulk diffusivity was attributed to a mechanism in which the Au atoms enter into the interstitial positions of the Sn lattice. The radius of a Sn ion in the lattice is considerably smaller than the atomic radius, i.e., only 0.59Å.[23] This is only 37% of the Au atomic radius and thus favorable to interstitial diffusion in Sn. This diffusion is 3−4 orders of magnitude faster than the self-diffusion of Sn.[24] Dyson[18] has studied the diffusion of gold in tin single crystals in the temperature range 135−225 °C using a radioactive tracer technique. By extrapolation we obtain diffusivities of Au in Sn at 22 °C of 4.0×10^{-11} cm^2 s^{-1} parallel to the c axis and 1.1×10^{-11} cm^2 s^{-1} parallel to the a axis, which gives diffusion lengths $(Dt)^{1/2}$ in 1 min of about 5000 and 80 Å, respectively, i.e., a very rapid diffusion of gold in tin. The growth orientation of the single-crystal tin section in the present study is along the a axis ([100]),[16] the diffusion layers in Figures 2 to 4 are about 100 to 300 nm, which is in good agreement with the diffusion length $(Dt)^{1/2}$ along the a axis from 2 to 24 h (the interval time from synthesis to TEM observation).

The diffusivity of tin in gold is considerably less than that of gold in tin, which is consistent with the fact that the diffusion of tin in gold takes place by the substitution (vacancy) mechanism. Dreyer et al.[25] have measured the diffusivity of tin in gold between 700 and 1000 °C. If we extrapolate these results to room temperature we obtain a diffusion length of 1.0×10^{-4} nm in 5 h and 2.2×10^{-4} nm

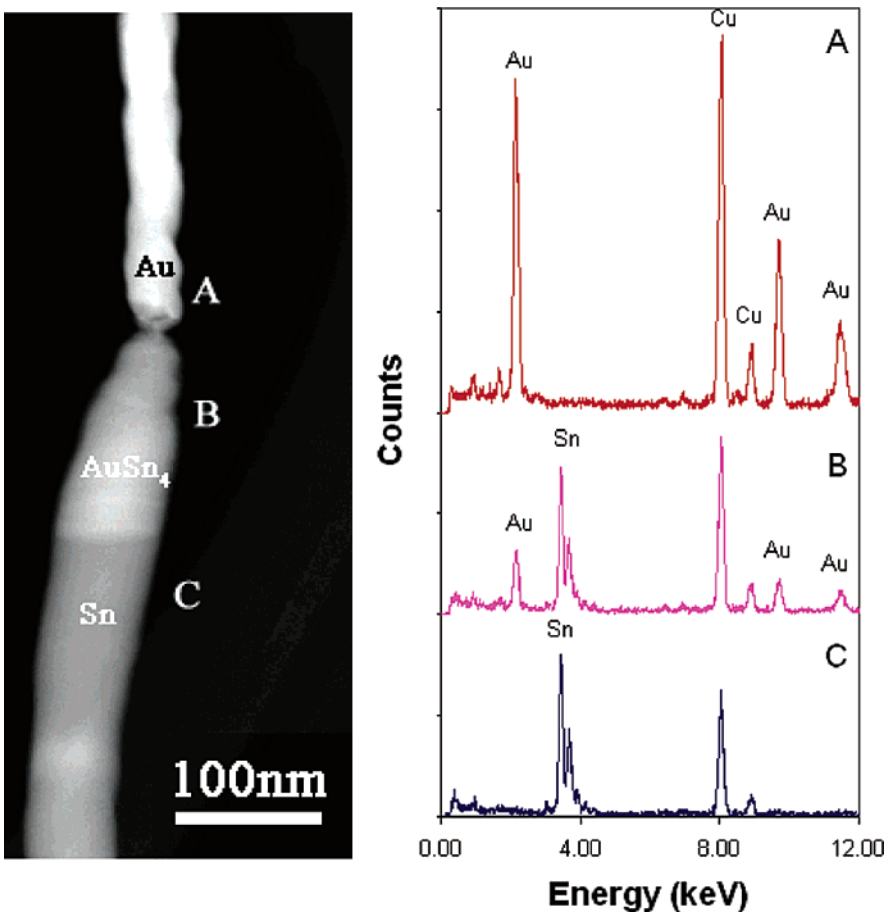

Figure 4. STEM ADF image and EDX analyses of a representative Au/$AuSn_4$/Sn/Au nanowire. The letters A, B, and C along the wire axis represent positions at which the EDX spectrum was recorded. Cu signals originated from the Cu TEM grid.

in 24 h. This means that tin in gold grains would be unobservable, which is in agreement with our observations.

The striking difference in diffusion layer structures between Au/Sn and Sn/Au might come from the thin tin oxide layer in the bottom Sn/Au junction. This oxide layer may act as a barrier layer to stop the bottom gold diffusion to the tin section, although we cannot rule out the possibility that this oxide layer forms after the wires are released from the membrane and exposed to air.

The growth of the AuSn and/or $AuSn_4$ layer is diffusion controlled. Using implanted argon ions as a Kirkendall marker, Gregersen et al.[19] have shown that at room temperature transport of gold through the AuSn phase is about 3 times faster than the transport of tin. This is consistent with the uneven cross-section of the junction nanowire, i.e., the fact that the AuSn compound section is much thicker than the Au section and slightly thicker than the Sn section.

Figure 5 shows the resistance versus temperature for the Au−Sn junction nanowires. A significant drop of the resistance near about 3.6 K was found, which was attributed to the superconducting transition of Sn nanowires. Below 3.6 K, two additional small drops were observed at 2.3 K and 1.2 K, respectively. Early studies show that all the Au−Sn intermetallic compounds become superconducting at low temperatures.[26] The drop at $T_c = 1.2$ K is likely due to the superconducting transition of AuSn intermetallic phase, while

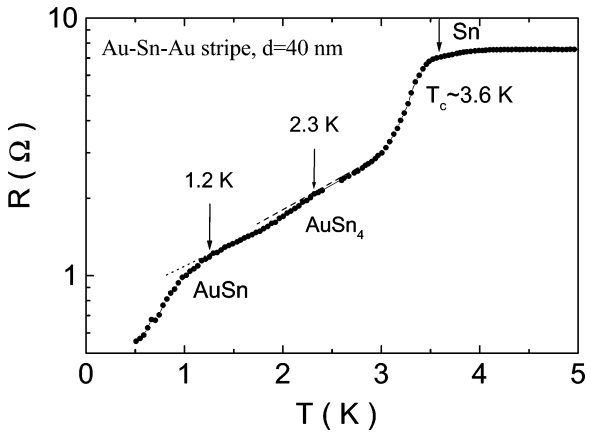

Figure 5. Resistance versus temperature for the Au−Sn junction nanowires measured with the PPMS system. The anomaly near $T_c = 3.6$ K is from Sn segments of the nanowires, while those near 1.2 and 2.3 K are possibly from AuSn and $AuSn_4$ intermetallic phases, respectively.

the weaker one at $T_c = 2.3$ K is from $AuSn_4$ intermetallic phase. We came to this conclusion because the superconducting transition temperature of AuSn was reported to be 1.25 K,[27] and the superconducting transition temperature of $AuSn_4$ was reported to be 2.4.[28] These transport data are in agreement with our structural identification. The residual resistance is from the Au leads and the contact resistance due to the two-probe configuration, while the broadening of

the phase transition might be due to the combination of size confinement of superconducting segments[16,29] and the proximity effect between superconducting segment and normal metal.[30] It has been shown that pure Sn nanowires exhibit broadening of phase transition and finite resistivity tail due to the quantum confinement effect when their diameters are less than 60 nm.[16,29,30] Weakness of superconductivity induced by proximity effect has been extensively studied in S/N bilayer system. It might be quite interesting to study the proximity effect Josephson system of Sn/AuSn/Sn or Sn/$AuSn_4$/Sn by controlling the length of Au wires so that the Au atoms were completely diffused into Sn to form the alloys, which may have potential promise in nanoscale superconducting electronic devices.[31]

In summary, we have synthesized Au/Sn/Au junction nanowires by a template electrodeposition method and have studied the relationship between microstructure and superconductivity by X-ray diffraction, HRTEM, STEM, EDS, and electrical transport measurements. Two intermetallic compounds, AuSn and $AuSn_4$ were observed at the top Au/Sn junction in the nanowires. The composition and structure of the Au/Sn and Sn/Au junctions were different, and the difference could be ascribed to the rapid diffusion of Au in Sn as well as the barrier of a thin oxide layer at the Sn/Au junction. Au/Sn/Au nanowires exhibit superconducting behavior and the superconducting transition temperatures of the AuSn and $AuSn_4$ segments were found to be 1.2 and 2.3 K, respectively.

Acknowledgment. This work is supported by a Seed Grant provided by Penn State Materials Research Institute and the Penn State MRSEC under NSF grants DMR 0080019 and DMR 0213623. T.E.M. thanks Prof. Paul Alivisatos for a helpful discussion of the Kirkendall effect in nanoparticles. TEM experiments were conducted at the Materials Research Institute TEM facility.

References

(1) Martin, C. R. *Science* **1994**, *266*, 1961−1966.
(2) Martin, C. R. *Chem. Mater.* **1996**, *8*, 1739−1746.
(3) Huczko, A. *Appl. Phys. A* **2000**, *70*, 365−376.
(4) Piraux, L.; George, J. M.; Despres, J. F.; Leroy, C.; Ferain, E.; Legras, R.; Ounadjela, K.; Fert, A. *Appl. Phys. Lett.* **1994**, *65*, 2482.
(5) Blondel, A.; Meier, J. P.; Doudin, B.; Ansermet, J.-P. *Appl. Phys. Lett.* **1994**, *65*, 3019.
(6) Gudiksen, M. S.; Lauhon, L. J.; Wang, J.; Smith, D. C.; Lieber, C. M. *Nature* **2002**, *415*, 617−620.
(7) Wu, Y.; Fan, R.; Yang, P. *Nano Lett.* **2002**, *2*, 83−86.
(8) Tian, M. L.; Wang, J. G.; Kurtz, J.; Mallouk, T. E.; Chan, M. H. W. *Nano Lett.* **2003**, *3*, 919.
(9) Sauer, G.; Brehm, G.; Schneider, S.; Nielsch, K.; Wehrspohn, R. B.; Choi, J.; Hofmeister, H.; Gösele, U. *J. Appl. Phys.* **2002**, *91*, 3243−3247.
(10) Gao, T.; Meng, G. W.; Zhang, J.; Wang, Y. W.; Liang, C. H.; Fan, J. C.; Zhang, L. D. *Appl. Phys. A* **2001**, *73*, 251−254.
(11) Glazer, J. *Int. Mater. Rev.* **1995**, *40*, 65.
(12) Bezryadin, A.; Lau, C. N.; Tinkham, M. *Nature* **2000**, *404*, 971.
(13) Lau, C. N.; Markovic, N.; Bockrath, M.; Bezryadin, A.; Tinkham, M. *Phys. Rev. Lett.* **2001**, *87*, 217003.
(14) Giordano, N. *Phys. Rev. Lett.* **1988**, *61*, 2137. Giordano, N. *Phys. Rev. B* **1990**, *41*, 6350. Giordano, N. *Phys. Rev. B* **1991**, *43*, *160*.
(15) Arutyunov, K. Y.; Ryynänen, T. V.; Pekola, J. P.; Pavolotski, A. B. *Phys. Rev. B* **2001**, *63*, 092506.
(16) Tian, M.; Wang, J.; Snyder, J.; Kurtz, J.; Liu, Y.; Schiffer, P.; Mallouk, T. E.; Chan, M. H. W. *Appl. Phys. Lett.* **2003**, *83*, 1620−1622.
(17) Wang, J.; Tian, M.; Mallouk, T. E.; Chan, M. H. W. *J. Phys. Chem. B* **2004**, *108*, 841−845.
(18) Dyson, B. F. *J. Appl. Phys.* **1966**, *37*, 2375−2377.
(19) Gregersen, D.; Buene, L.; Finstad, T.; Lonsjo, O.; Olsen, T. *Thin Solid Films* **1981**, *78*.
(20) Nakahara, S.; McCoy, R. J. *Thin Solid Films* **1980**, *72*, 457−461.
(21) Buene, L.; Falkenberg-Arell, H.; Tafto, J. *Thin Solid Films* **1980**, *67*, 95−102.
(22) Walser, R. M.; Bene, R. W. *Appl. Phys. Lett.* **1976**, *28*, 624−625.
(23) Harrison, W. A. *Electronic structure and the properties of solids: the physics of the chemical bond*; Dover Publications: New York, 1989.
(24) Tu, K.-N.; Rosenberg, R. *Jpn. J. Appl. Phys.* **1974**, *Suppl. 2, Part 1*, 633−636.
(25) Dreyer, K., Herzig, C., Heumann, T., Lodding, A., Lagerwall, T., Eds.; *Zeitschrift für Naturforschung*; *Tübingen: Verlag der Zeitschrift für Naturforschung*; Marstrand, Sweden, 1971; p 237.
(26) Okamoto, H.; Massalski, T. B. *Phase diagrams of binary gold alloys*; ASM International: Metals Park, Ohio, 1987.
(27) Hamilton, D. C.; Raub, C. J.; Matthias, B. T.; Corenzwit, E.; Hull, G. W., Jr. *J. Phys. Chem. Solids* **1965**, *26*, 665−667.
(28) Allen, J. F. *Philos. Mag.* **1933**, *16*, 1005−1044.
(29) Tian, M. L.; Wang, J. G.; Snyder, J.; Kurtz, J.; Schiffer, P.; Liu, Y.; Mallouk, T. E.; Chan, M. H. W. *Phys. Rev. Lett.* **2004**, submitted.
(30) Courtois, H.; Gandit, P.; Pannetier, B. *Phys. Rev. B* **1995**, *52*, 1162−1166.
(31) van Dover: R. B.; de Lozanne, A.; Beasley, M. R. *J. Appl. Phys* **1981**, *52*, 7327−7342.

NL0492988